Astron. Astrophys. 186, 241–254 (1987)

ASTRONOMY AND ASTROPHYSICS

Rotational modulation and flares on RS CVn and BY Dra stars

IV. The spatially resolved chromosphere of AR Lacertae★

F.M. Walter[1], J.E. Neff[2], D.M. Gibson[3,★★], J.L. Linsky[2,★★★,★★★★], M. Rodonò[4,★★★★], D.E. Gary[5,★★], and C.J. Butler[6]

[1] Center for Astrophysics and Space Astronomy, University of Colorado, Boulder, CO 80309-0391, USA
[2] Joint Institute for Laboratory Astrophysics, University of Colorado, Boulder, CO 80309-0440, USA
[3] Astrophysics Research Center and Department of Physics, New Mexico Institute of Mining and Technology, Socorro, NM 87801, USA
[4] Istituto di Astronomia, Città Universitaria, Viale A. Doria 6, I-95125 Catania, Italy
[5] Solar Astronomy, 264-33, Caltech, Pasadena, CA 91125, USA
[6] Armagh Observatory, Armagh BT61 9DG, Northern Ireland

Received November 17, 1986; accepted April 27, 1987

Summary. We observed the RS Canum Venaticorum system AR Lacertae systematically over an orbital period with the International Ultraviolet Explorer in October 1983. Contemporaneous radio observations were obtained at the Very Large Array (VLA). The spectra of the Mg II k emission line were analyzed using a Doppler imaging technique. In this way, we identified three discrete regions of emission in the outer atmosphere of the K star – two "plages" and a chromospheric brightening that was related to a radio flare. The widths of the plage profiles indicate that the two plages together cover about 2% of the visible stellar hemisphere, and their $v \sin i$ values indicate that they lie close to the equator of the K star. The Mg II k surface flux in the plages is about five times the mean Mg II k surface flux of the K star. We then used the far-ultraviolet spectra obtained at the eclipse phases to separate the individual contributions of the two stars and the plage and flare regions in order to estimate their line surface fluxes.

Key words: stars: atmospheres of – stars: chromospheres of – stars: binaries: spectroscopic – stars: AR Lacertae – stars: radio radiation of

1. Introduction

Stellar atmospheres have traditionally been modelled as homogeneous, plane-parallel or spherically-symmetric layers. In such single-component atmospheres the local physical parameters depend only upon radial position. The Sun, however, has dark sunspots, magnetic loops, and a variety of other structures at all levels from the photosphere through the corona and on all observable scales (e.g., Eddy, 1979). If solar analogy, the initial assumption in studies of the "solar-stellar connection", is to be applied to other late-type stars, then realistic stellar atmosphere models must include temperature and density inhomogeneities analogous to those that exist on the Sun.

We stress the word analogous because observations of late-type stars indicate that some stars are far more active than the Sun. For example, many active dwarfs and subgiants have dark regions (starspots) that cover as much as 20% of their photospheres (e.g., Vogt, 1983; Rodonò, 1983; Poe and Eaton, 1985), compared to the less than 0.1% surface coverage of sunspots (Bray and Loughhead, 1965). The ultraviolet emission line fluxes observed in many active late-type stars can not be explained even by complete surface coverage of solar-like active regions (Simon et al., 1985). To account for this extreme level of activity one is led to hypothesize (a) continuous low-level flaring, (b) emission from solar-like structures but at much higher pressures than observed on the Sun, or (c) completely new types of surface structures. In order to determine the physical conditions within these regions we need to determine their relative surface area coverages and the spectra of the individual regions.

There are several techniques that can be used to identify and study discrete atmospheric structures (which for convenience we call plages if brighter than the surrounding atmosphere and spots if darker). One technique, *rotational modulation*, is to associate the variation in stellar flux in a given passband with the passage of regions of contrasting brightness across the visible hemisphere as the star rotates. Many observers (e.g., Eaton and Hall, 1979; Hall, 1981; Poe and Eaton, 1985; Rodonò et al., 1986, Paper I) have studied the broad-band optical light curves of RS Canum Venaticorum systems and active dwarfs to determine the surface coverage of dark spots in their photospheres. Variations in the intrinsic colors have been used to derive the spot sizes and temperatures, while asymmetries in the light curve have been used to constrain the number and shape of discrete photospheric spots. Marstad et al. (1982; see also Rodonò et al., 1987, Paper III)

Send offprint requests to: J.E. Neff

★ Based on observations collected with IUE at the ESA Satellite Tracking Station, Villafranca (Spain) and NASA Goddard Space Flight Center, Greenbelt, MD (USA).
★★ Visiting Astronomer, VLA. The VLA of the National Radio Astronomy Observatory is operated by Associated Universities, Incorporated, under contract to the National Science Foundation.
★★★ Staff Member, Quantum Physics Division, National Bureau of Standards.
★★★★ Guest Observer, the International Ultraviolet Explorer.

found a bright transition region plage on the RS CVn star II Pegasi and Byrne et al. (1987, Paper VI) estimated its area using the rotational modulation of far-ultraviolet line fluxes. Linsky et al. (1984) and Byrne et al. (1987) used these observations to construct two-component atmospheric models for II Peg. However, rotational modulation provides information along only one dimension (projected longitude). Longitudes are determined from timing the appearance and disappearance of discrete features over the stellar limb, and extents of the features are estimated from the shape of the light curve. Further, the absence of rotational modulation does not imply the absence of discrete regions of enhanced contrast. Only a highly nonuniform distribution of regions of greatly enhanced contrast will produce a rotational modulation in the disk-averaged light.

A second technique is to use the *occultation* of stars in an eclipsing binary system. Discrete surface structures produce observable deviations in the light curve obtained during an eclipse. We have applied this technique to AR Lac to deduce its coronal structure from X-ray observations (Walter et al., 1983, hereafter WGB), and its photospheric structure from optical photometry (Rodonò, 1986).

One would like to obtain an image of the stellar chromosphere and transition region. Unfortunately stellar surfaces can not be imaged directly, except perhaps by applying speckle interferometry to the stars with the largest apparent diameters (e.g., Soderblom, 1985). However, a third technique, *Doppler imaging*, can be used to construct such an image. In this technique, the position of a discrete component on a spectral line profile that is broadened mainly by rotation is used to determine the distance of that component from the rotational axis on the projected stellar disk. If the inclination of the rotation axis is known, then this distance, when followed over the entire orbital cycle, provides both the latitude and longitude of that feature on the stellar surface. In order to construct an image, the shape of the feature must also be determined from the spectral width of the feature and from details of the light curve.

Vogt and Penrod (1983) applied a Doppler imaging technique to map the dark photospheric structures (starspots) on HR 1099. Their technique involved a detailed synthesis of composite absorption line profiles using the relative brightnesses of the spot and photosphere as input to the model. In this paper, we describe a Doppler imaging technique that allows us to determine the relative brightnesses and areas of discrete regions in the *chromospheres* of active, late-type stars.

In order to apply our Doppler imaging technique, high-resolution ultraviolet spectra must be obtained at many phases throughout an orbital cycle. We obtained such observations of AR Lacertae in October 1983. The results of the Doppler imaging analysis, coupled with observations at other wavelengths, allow us to map the chromospheres of the AR Lac system at this epoch. Using this map, we are able to model each emission component separately (Neff et al., 1986a).

2. The AR Lacertae system

AR Lacertae (HD 210334; HR 8448) is the brightest ($V = 6.1$) known eclipsing RS CVn system. In this paper we use the system parameters (Table 1) given by Chambliss (1976). AR Lac is composed of two active, evolved stars – a G2 subgiant located about 1 mag above the main sequence and a K0 subgiant located about 2.5 mag above the main sequence. The system has a semi-major axis of 9.1 $R_\odot$, an inclination of 87°, and an orbital period of 24 min less than 2 days. The G subgiant is totally eclipsed for 2.1 h at primary minimum; secondary eclipse is annular, with 30% of the K star occulted. The K star has nearly four times the surface area of the G star, is more massive (but by less than 1%), and has a bolometric luminosity of about 0.5 mag brighter than that of the G star. Both stars rotate nearly synchronously with the orbital period.

Table 1. AR Lacertae system parameters

Property	G2 IV star	K0 III–IV star	Units
Mass	1.35	1.36	$M_\odot$
Radius	1.54	2.82	$R_\odot$
$v \sin i$	40	72	km s^{-1}
K	116.1	115.6	km s^{-1}
V	6.94	6.75	Magnitudes
$B - V$	0.68	0.93	Magnitudes

The G component of AR Lac was the first star for which dark starspots were proposed to explain photometric irregularities during the eclipses (Kron, 1947). Some of the observed irregularities, however, were due to a variable comparison star (Blanco and Catalano, 1970), the long-period RS CVn system HK Lac. Although AR Lac is one of the original members of the RS CVn class (Hall, 1976; Popper and Ulrich, 1977), it is atypical of this class in that both stars are somewhat evolved and both exhibit strong stellar activity. AR Lac is an ideal system for an investigation of stellar activity and stellar surface inhomogeneities for the following reasons:

(1) The system is bright and eclipsing.

(2) The stellar lines are broad because of the nearly synchronous rotation, with $v \sin i = 72$ and 40 km s^{-1} for the K and G stars, respectively. Rotationally broadened lines are required for Doppler imaging techniques.

(3) The emission lines from the two stars are easily separated at moderate spectral resolution, since the maximum radial velocity difference is 232 km s^{-1} (Batten et al., 1978). Even at first contact the projected stellar orbital velocities differ by about 100 km s^{-1}.

(4) Both stars are active.

In addition, we are dealing with stars of the same age, rotational period, and nearly identical masses, but in somewhat different evolutionary states. The system may therefore provide some clues to the dependence of stellar activity on evolution.

For these reasons, AR Lac has been the subject of many studies in the past. Naftilan and Drake (1977) and Naftilan and Aikman (1981) discussed the optical spectra and the behavior of the Ca II H and K emission lines. The system is a variable radio source (Gibson and Hjellming, 1974; Owen and Gibson, 1978) as well as a bright X-ray source (Walter et al., 1980). From an analysis of *Einstein* SSS data, Swank et al. (1981) deduced a two temperature component model for the X-ray corona. WGB observed the X-ray eclipses and deduced the geometrical structure of the corona.

The ephemeris of the system (zero phase = primary eclipse), based on photometry in 1981 and 1982 (Paper I), is JD 2444977.0216 + 1.983170E. Due to the variation of the or-

bital period, phases computed using this ephemeris are 0.014 larger than those computed from the ephemeris of Hall (1981).

3. Observations and analysis

The ultraviolet spectra were obtained on 3–5 October 1983 using the *International Ultraviolet Explorer* (IUE; see Boggess et al., 1978). We obtained eight long-wavelength (LWR) spectra of the Mg II *h* and *k* lines with about 0.20 Å resolution, and nine low-resolution (6 Å), short-wavelength (SWP) spectra. The data were reduced at the Colorado Regional Data Analysis Facility (RDAF) by applying the standard flux calibrations (Cassatella, et al. 1982; Bohlin and Holm, 1980). The starting times of these observations, orbital phases, and exposure durations are given in Table 2.

In support of the IUE observations, we obtained 12 h of VLA observations at 2, 6, and 20 cm on 4 and 5 October 1983. Ground-based photometry was obtained at several sites over a several month period bracketing our other observations. The photometry and spot-modeling results will be presented in a later paper in this series (Cutispoto et al., in preparation).

3.1. *Line profile fitting technique*

All line profile and line flux measurements were made at the Colorado RDAF by fitting the spectral lines with a specified number of gaussian profiles (one to five) and the background with a quadratic function. The fitting program is based upon the CURFIT program (Bevington, 1969), which uses the Marquardt algorithm to minimize the chi-square of the fit. In practice, all parameters (three for the quadratic background plus three for each gaussian profile) were allowed to vary. Initial estimates can be input interactively. Alternatively, results from a previous fit can be used as initial estimates, allowing interactive changes to be made in any parameter before proceeding with the subsequent fit.

Although our fitting program can be used with any assumed analytic profile, we have found that gaussian profiles provide an acceptable description of both the low-resolution SWP and high-resolution LWR emission lines. The SWP spectra are unresolved, and their profile is therefore instrumental. By using a gaussian fit, we can determine the SWP fluxes far more consistently than by simply integrating the flux between two arbitrary base points, primarily because the continuum level is set by a fit to many background points well removed from the line.

The intrinsic Mg II *h* and *k* line profiles, in the absence of stellar rotation, presumably have central reversals, and the line widths are likely given by the Mg II analog of the Wilson-Bappu relation (Ayres, 1980; Stencel et al., 1980). However, stellar rotation is expected to "fill in" the central reversal and enhance the Doppler emission core (Bielicz et al., 1985). Also, IUE has a very limited dynamic range, so it is likely that the exposure times appropriate to optimally expose the emission core will not be sufficient to detect any emission far in the (perhaps non-gaussian) line wings. For more deeply exposed spectra, however, this might not be the case. Finally, the stellar line profile is convolved with the IUE instrumental response. The net result is an observed line profile that is effectively gaussian.

We stress that Doppler imaging techniques, to be useful for determining the physical conditions within the discrete region, must provide more information than just the *location* of discrete regions. If the goal is to determine the physical properties of that region, its size and spectrum must first be determined. We further emphasize that a casual inspection of "bumps and wiggles" in the line profile is not sufficient to construct a Doppler image. The observed profile is a composite of many profiles formed in regions of different atmospheric structure and emanating from different positions on the visible disk. Only under special circumstances (i.e., a very narrow line superposed on a very broad line) do two line profiles add in such a way that the position of the resulting bump is the same as the position of one of the components.

Table 2. Log of IUE observations

Image	Resolution	Exposure start time (1983 UT) d	h	min	Exposure time (min)	Phase of mid exposure
LWR 16916	HIGH	276	21	39	50	0.88
LWR 16917	HIGH	277	00	06	42	0.93
LWR 16918	HIGH	277	02	16	45	0.97
LWR 16922	HIGH	277	12	27	55	0.19
LWR 16925	HIGH	278	01	06	45	0.45
LWR 16926	HIGH	278	03	43	55	0.51
LWR 16927	HIGH	278	06	09	55	0.56
LWR 16928	HIGH	278	08	37	45	0.61
SWP 21222	LOW	276	20	13	80	0.85
SWP 21223	LOW	276	22	36	80	0.90
SWP 21224	LOW	277	00	52	80	0.95
SWP 21225	LOW	277	03	05	80	0.00
SWP 21230	LOW	277	13	27	80	0.21
SWP 21234	LOW	278	01	56	100	0.50
SWP 21235	LOW	278	04	43	80	0.53
SWP 21236	LOW	278	07	10	80	0.59
SWP 21237	LOW	278	09	31	60	0.64

3.2. *LWR spectra*

The eight LWR spectra commence at orbital phase $\phi = 0.88$ and provide phase coverage around a single orbit, although five of the spectra were obtained within one tenth of a phase of either primary or secondary minimum. As we justify below, the Mg II *k* spectrum obtained at $\phi = 0.19$ (see Fig. 1) is composed of two broad emission components, an absorption feature on the blueward side of the red emission component, and a small emission feature on the redward side of the same emission component. We attribute the broad emission components to the global chromospheric emission of the G and K stars (the blue and red components, respectively). The absorption feature is interstellar; its width indicates the instrumental resolution. We attribute the small emission feature on the red edge of the K star Mg II *k* line to a region of enhanced emission on the leading hemisphere of the K star, Plage B, which we discuss in detail in Sect. 4.1.

These details that we ascribe to the line profile shown in Fig. 1 were identified only after a careful analysis of the spectra. We applied an iterative method that employed a minimum number of assumptions in each step, and we selected improvements *a posteriori* based not upon a better match to the line profile but, more importantly, upon a better reproduction of those well determined aspects of the system (e.g., projected stellar radial velocities).

As an initial step, it was obvious that at least two components are required to match the profiles. We first fit the profiles with one emission plus one absorption component and, alternatively, with two emission components. The former yielded unacceptable fits to the profiles and two components of widely varying position and width. The latter gave a good first-order approximation to the line profiles and is consistent with emission from both stars in the system. However, there was always an additional, narrow absorption feature, which we then fit with a third component (using the original 2 component fit as an initial estimate). This resulted in an unresolved absorption line at the same wavelength in each spectrum, which we attribute to interstellar absorption.

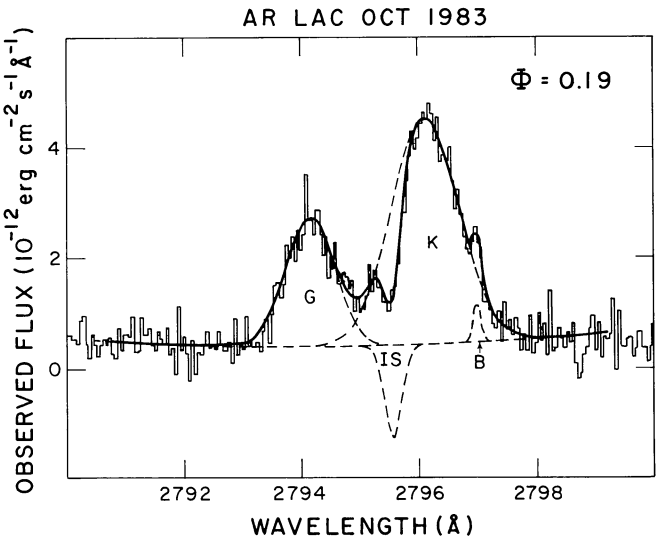

Fig. 1. The Mg II *k* line profile of AR Lac at $\phi = 0.19$ with a 4 component fit (the G and K stars, the interstellar absorption, and Plage B) superposed on a quadratic background. The histogram is the observed profile, and the heavy line is the resultant (sum) fit of the 4 components (dashed lines)

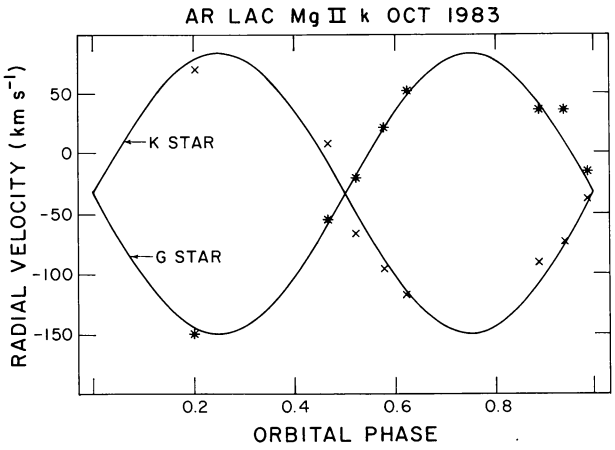

Fig. 2. The predicted radial velocities of the G and K stars (solid lines) using elements from Batten et al. (1978). The measured K star velocities are the crosses, while the measured velocities of the G star are denoted by asterisks. Notice that we did not force *exact* agreement with the predicted positions, but rough agreement was the primary motivation for the addition of Plage A

Since the optical depth of the interstellar medium in a given line of sight is constant, the equivalent width of this feature can be assumed to remain constant. Before adding any additional components to these fits, we plotted the line centroids, widths, and fluxes against phase, using the mean interstellar position as a velocity fiducial. Most of the measured emission line positions agreed with the expected (and well known) stellar velocities. However, at several phases the only way to make the global stellar line profile match (within $\sim 10\,\mathrm{km\,s^{-1}}$) its expected position was to add a fourth component to the fit. Furthermore, the line widths and fluxes were anomalously high at these phases. We therefore added an extra component onto the global K star profile. Figure 2 shows the centroid velocities of the resultant fits along with the projected stellar radial velocities. With four components we were able to adequately represent the global features of the line profiles. However, a narrow component was then seen in the residual spectrum at several phases. We fit this feature with a fifth component and found that the inferred position on the surface of the K star, its measured line width, and its line flux are constant. We therefore assert that our multiple-component fits provide the simplest accurate representation of the observed line profiles. The final fits are presented in Fig. 3 and summarized in Table 3. Using these fits, we were able to determine the following characteristics of the AR Lac system:

(1) The systemic velocity is $-30 \pm 8\,\mathrm{km\,s^{-1}}$ (measured from the six spectra furthest removed from mid-eclipse; the uncertainty is the standard deviation of the individual measurements), in excellent agreement with the published values of $-33.7\,\mathrm{km\,s^{-1}}$ (Batten et al., 1978) and $-35\,\mathrm{km\,s^{-1}}$ (Hoffleit, 1982).

(2) The mean measured wavelength of the interstellar absorption line, 2795.52 ± 0.04 Å, corresponds to a heliocentric interstellar medium velocity of $+2 \pm 5\,\mathrm{km\,s^{-1}}$ in the line of sight towards AR Lac. Böhm-Vitense (1981) and Crutcher (1982) predict a mean interstellar medium velocity of $+5\,\mathrm{km\,s^{-1}}$ and $-8\,\mathrm{km\,s^{-1}}$, respectively, in this line of sight. Using the measured wavelength of the interstellar line as a fiducial mark, the IUE velocity scale during the course of these observations was stable to better than about $\pm 3\,\mathrm{km\,s^{-1}}$.

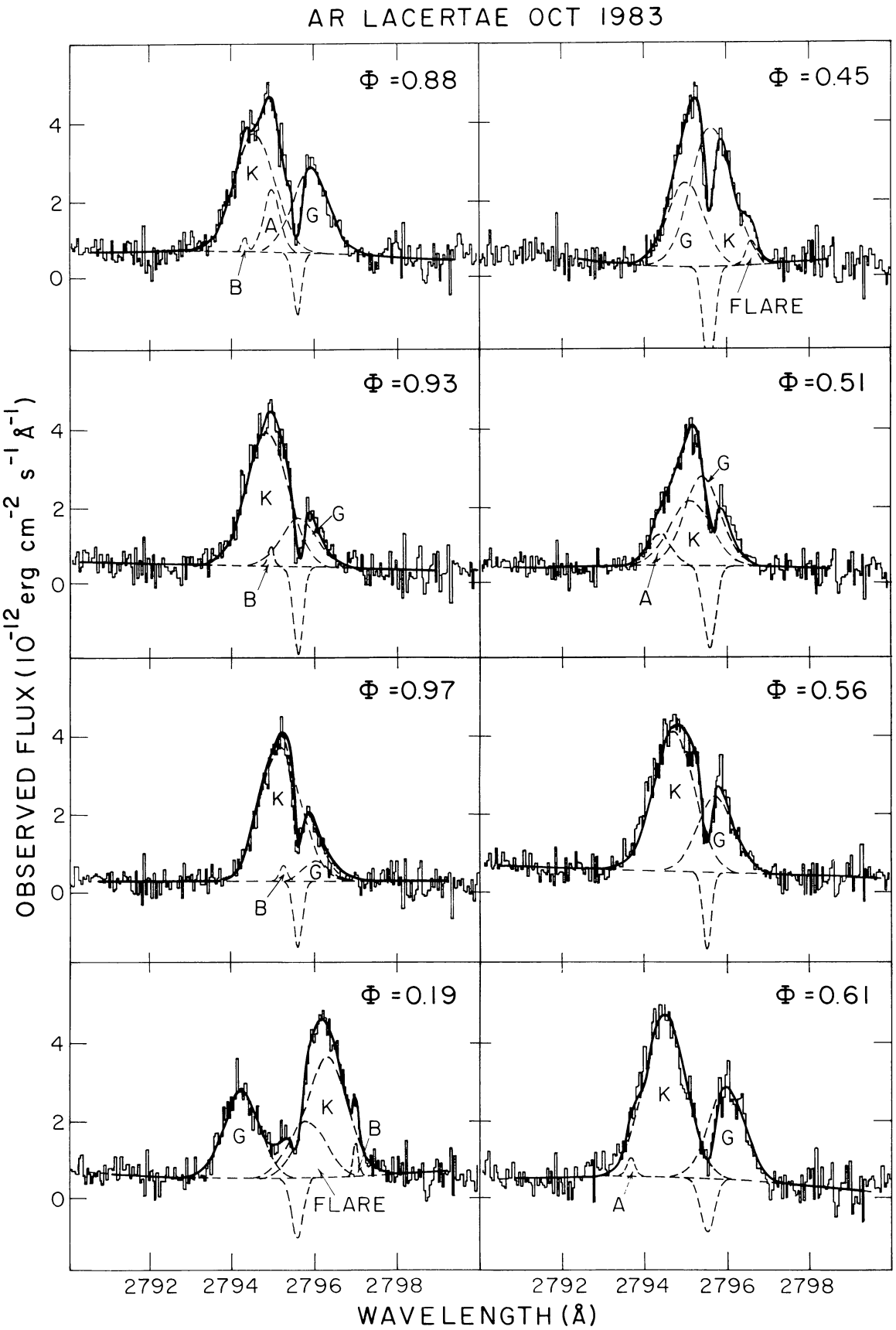

Fig. 3. All 8 observed Mg II *k* line profiles (histograms) with fits superposed. The heavy solid lines are the sum of the 4 or 5 gaussian components

Table 3. Observed Mg II k line fluxes (10^{-12} erg cm^{-2} s^{-1})

Image	Phase	K star	G star	Plage A	Plage B	Flare
16916	0.88	4.0	2.3	0.82	0.06	–
16917	0.93	4.6	0.9	0.60[a]	0.12	–
16918	0.97	>4.3[b]	<0.4[c]	??[d]	0.08	–
16922	0.19	4.4	2.4	–	0.12	1.3
16925	0.45	4.5	2.5	–	–	0.4
16926	0.51	2.6	2.5	0.37	–	–
16927	0.56	4.4	2.2	<0.1	–	–
16928	0.61	5.4[e]	2.5	0.14[e]	–	–

[a] Estimated by constraining the equivalent width of the interstellar absorption to remain constant.
[b] Lower limit due to line blending problems near primary eclipse.
[c] Upper limit due to line blending problems near primary eclipse.
[d] Unmeasurable due to proximity to interstellar absorption and line blending problems near primary eclipse.
[e] Lower limit on plage flux; upper limit on K star flux. Flux indicates that the plage is present, but it is not seen as a discrete feature on the line profile.

(3) Using the six observations outside of eclipse, we were able to measure the epoch of zero phase independently of the photometric determination. The radial velocity data are in excellent agreement with the photometrically determined ephemeris, giving a best fit phase offset of -0.004 ± 0.006. Based on these radial velocity data alone, any uncertainty in the ephemeris at the time of observation is likely to be less than 15 min and is therefore negligible relative to the integration times (typically 45 min) of the IUE spectra.

(4) We have used the outside-of-eclipse fits to determine mean amplitudes and widths of the global stellar emission components. Outside of eclipse, the mean widths (FWHM) of the quiescent emission line with the instrumental width deconvolved are 76 ± 5 and 87 ± 5 km s^{-1} for the G and K stars, respectively. These line widths are in good agreement with those predicted by convolving the stellar rotation with the intrinsic line width predicted from the Mg II analog of the Wilson-Bappu relation (Stencel et al., 1980), which, for a stellar luminosity corresponding to a distance of 40 pc, predicts line widths of 68 and 91 km s^{-1} for the G and K star, respectively.

(5) The fluxes in the various components are plotted in Fig. 4. The mean flux observed from the G star was fairly constant at $2.5 \pm 0.5\,10^{-12}$ erg s^{-1} cm^{-2}, corresponding to a Mg II k line surface flux of $3.0\,10^{6}$ erg s^{-1} cm^{-2}. Primary eclipse ($\phi = 0$) is evident in the G star light curve. The K star flux showed significantly more variability, primarily between phase 0.97 and phase 0.19, when it increased by about 50%. We attribute the large increase in flux from the K star at phase 0.19 to a transient brightening associated with the radio flare discussed below and the high levels prior to the flare and at $\phi = 0.61$ to a large plage. The mean flux observed from the K star, omitting the eclipses and the plage components, is $4.5 \pm 0.5\,10^{-12}$ erg s^{-1} cm^{-2}, corresponding to a Mg II k line surface flux of $2.1\,10^{6}$ erg s^{-1} cm^{-2}. The observed fluxes in the G and K stars are quite uncertain at phases 0.97 and 0.51 due to the eclipses.

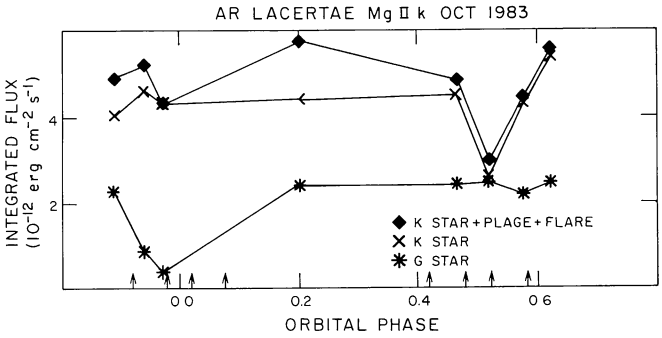

Fig. 4. The observed Mg II k line flux versus time. The global fluxes of the G and K stars, and the total K star flux (including the plages and the flare) are indicated. The arrows indicate the phase of the 1st through 4th contacts for both the total ($\phi = 0.0$) and annular ($\phi = 0.5$) eclipses. Primary eclipse ($\phi = 0.00$) is evident in the G star light curve; the dip in the K star light curve at $\phi \sim 0.50$ is due to the annular eclipse. Notice the variation in the plage flux (primarily due to Plage A) between $\phi = 0.88$ and the end of the observations ($\phi = 0.61$). See also Table 3. The K star flux is a lower limit, and the G star flux an upper limit, at $\phi = 0.97$ due to line blending. The K star flux at $\phi = 0.61$ is likely overestimated because the plage is not spatially resolved at this phase

We have measured all of the Mg II h lines in a similar fashion. The h lines lie well down on the echelle blaze and hence are less well exposed than the k lines. The shape of the h line is identical to that of the k line at the same phase. A comparison of the h and k lines at phase 0.88 is shown in Fig. 5. All departures between the profiles are 3 points or less in width (the unresolved interstellar absorption feature is 5 points FWHM).

We estimate that the formal uncertainties in the measured stellar velocities are less than 6 km s^{-1}. However, there could be small systematic errors if the true line shapes are not gaussian, since the wavelengths are determined by fitting the entire line

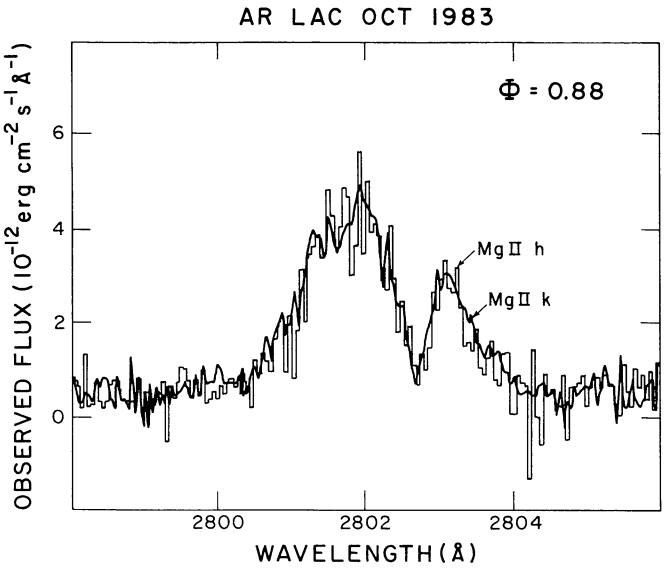

Fig. 5. The Mg II *h* line profile (histogram) at $\phi = 0.88$, illustrating its similar line shape but poorer S/N than the *k* line. The solid line is the *k* line profile shifted in wavelength. At all phases, multiple-component fits to the *h* lines agreed in detail with those to the *k* lines. The instrumental resolution is 5 points

profile. The absolute uncertainties in the measured flux depend on the uncertainties in the IUE calibration (10 to 20%), but the relative flux measurements are more accurate ($\lesssim$10%).

We have identified two discrete regions of emission (plages) on the K star. We will refer to these features as Plage A and Plage B.

Plage A is the cause of the asymmetry seen between the K star *k* line (henceforth the K*k* line) center and the interstellar absorption feature at phase 0.88 (Fig. 3). The emission from Plage A is completely absorbed by interstellar Mg II at $\phi = 0.97$. It is likely seen reappearing over the blue limb between phases 0.51 and 0.61, but the strongest evidence for reappearance is the increasing line flux, because the discrete plage component in the line profile is only marginally detected. This plage component appears to be spatially extended, as the velocity half width of the component at $\phi = 0.88$ is about 20 km s^{-1} (the instrumental full width resolution is about 25 km s^{-1}).

Plage B is evident as the small emission peak on the redward wing of the K*k* line at $\phi = 0.19$. It can be seen blueward of the K*k* peak at $\phi = 0.88$ and 0.93 (Fig. 3), and it might be present at the edge of the interstellar absorption at $\phi = 0.97$. The plage was not on the visible hemisphere between phases 0.45 and 0.61. The deconvolved Doppler width of the emission from this plage is consistent with the instrumental resolution (i.e., $\lesssim$15 km s^{-1}). The velocity of the feature is consistent with the emission being localized near stellar longitude 345° ± 5°, where the longitude of the central meridian is defined as 360° times the phase. Since the inclination is very close to 90°, projection may be ignored.

There is also a prominent emission feature seen on the red wing of the K*k* line at $\phi = 0.45$. This is likely due to the decay of a chromospheric flare that is responsible for the enhanced flux at $\phi = 0.19$. We will discuss the flare and the two plage regions further in Sect. 4.

3.3. *SWP specta*

We summarize the low-resolution SWP fluxes in Table 4 and Fig. 6. Given the low resolution of the SWP spectra, it is not possible to separate the contributions due to the two stars by

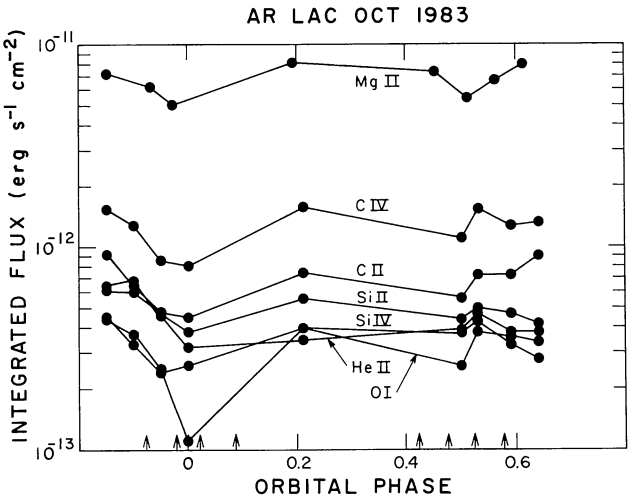

Fig. 6. The observed SWP line fluxes as a function of time, plotted against orbital phase. All flux measurements were made by fitting gaussians to the low-resolution profiles. The fluxes at $\phi = 0.00$ can be attributed to the K star alone. At all other phases, the flux includes the G star, K star, plage, and (at $\phi = 0.21$) flare contributions. The observations began at $\phi = 0.85$, and there was no phase overlap. As in Fig. 4, the phases of 1st through 4th contact are indicated by arrows. See also Table 4

Table 4. Observed SWP line fluxes (10^{-13} erg cm^{-2} s^{-1})

Image	Phase	N V 1240	O I 1305	C II 1335	Si IV 1396 + 1402	C IV 1550	He II 1640	Si II 1808 + 17	Si III 1893
21222	0.85	3.1	4.5	9.2	4.4	15.4	6.4	6.1	1.2
21223	0.90	2.1	3.3	6.5	3.7	12.8	6.8	6.0	1.0
21224	0.95	2.6	2.4	4.8	2.5	8.6	4.6	4.7	0.4
21225	0.00	1.8	2.6	4.5	1.1	8.1	3.2	3.8	1.0
21230	0.21	3.1	4.0	7.5	4.0	15.9	3.5	5.6	1.1
21234	0.50	2.2	2.6	5.6	3.8	11.1	3.9	4.4	0.8
21235	0.53	2.6	3.8	7.3	4.3	15.5	4.7	5.0	1.2
21236	0.59	2.3	3.6	7.3	3.3	12.8	3.8	4.7	0.8
21237	0.64	2.1	3.4	9.1	2.8	13.3	3.8	4.2	0.8

Table 5. Derived fluxes of the individual components[a]

Line	f_K	f_G	F_K[b]	F_G	f_P	F_P[c]	F_P/F_K	(F_P/F_K)[d]
N v	1.8	0.9	0.8	1.1	0.4	9.0	11.3	51.1
O i	2.6	0.8	1.2	1.0	1.2	27.0	22.6	136.4
C ii	4.5	2.5	2.1	2.9	2.3	53.8	26.0	200.0
Si iv	1.1	3.0	0.5	3.6	0.3	5.8	11.1	61.0
C iv	8.1	5.4	3.7	6.4	2.1	48.3	12.9	57.6
He ii	3.2	1.7	1.5	2.0	1.6	37.9	25.9	179.3
Si ii	3.8	1.7	1.8	2.0	0.7	15.0	8.6	41.4
Si iii	1.0	0.1	0.4	0.1	0.1	3.2	7.4	34.3
Mg ii (k)	45	25	21	30	3[e]	92	4.4	–
Mg ii (k)					1[f]	>92	>4.4	–

Observed line fluxes (f) are in units of 10^{-13} erg cm^{-2} s^{-1}.
Surfaces fluxes (F) are in units of 10^{5} erg cm^{-2} s^{-1}.
[a] Assuming $R = 0$, Eq. 1.
[b] Calculated with 98% filling factor.
[c] Calculated with 2% filling factor.
[d] Assuming $R = 1$, Eq. 1.
[e] Plage A only.
[f] Plage B only.

using their relative Doppler shifts. However, the constraints imposed by the fluxes observed during eclipse, together with those imposed by requiring consistency with the Mg II Doppler imaging results, do permit us, in principle, to determine the contributions of the individual stars.

We assumed that the flux measured during primary eclipse (SWP 21225) can be attributed to the global emission from the K star plus some emission from the plage regions (Plage A is near the limb at primary eclipse and Plage B should contribute a negligible fraction of the total flux). Similarly, we assumed that the flux measured at secondary eclipse (SWP 21234) is the sum of the G star flux plus a fraction of the K star flux determined at primary minimum. We would not expect to see any emission from the plages at this phase, since they would not be on the visible surface. With these two fluxes, it is possible to infer the plage and flare contributions if we assume that the global fluxes, like the Mg II emission, remained constant between the eclipses. A low level of Mg II variability, however, does not guarantee that the hotter (and probably optically thin) lines also remain steady.

If F_t, F_a, and F_p are the line fluxes measured during the primary (total) eclipse, secondary (annular) eclipse, and the spectrum obtained when both plage regions were roughly centered on the visible disk ($\phi = 0.87$), then to a first approximation

$$F_t \cong (1 - f)K + RP, \tag{1a}$$

$$F_a = G + (0.70)K, \tag{1b}$$

and

$$F_p = (1 - f)K + P + G, \tag{1c}$$

where K and G are the global fluxes from the K and G stars and P is the flux due to both plages. We take the total filling factor, f, for both plages to be 0.02, based on the sum of the Mg II k plage filling factors (see Sect. 4.1). The ratio of the flux observed from the plages when they are near the limb to that when they are near disk center is given by R. If the plages are optically thin, we expect $R \approx 1$. The actual value of R for large stellar active regions must be determined by future Doppler imaging studies. Although we expect R to be near 1, we have set $R = 0$, because this yields a *minimum* plage spectrum. Increasing R increases the emission line flux in the inferred plage spectrum at the expense of the K star spectrum. The fraction of the K star flux that is eclipsed, 0.30 using only the geometrical obscuration, might be overestimated near mid-eclipse and underestimated when one limb is eclipsed if the chromosphere and transition region are limb brightened.

Using these assumptions we solved Eq. (1) for K, G, and P to yield the surface fluxes in the three components (Table 5). In most lines, the surface fluxes of the two stars are roughly comparable (cf. WGB and Paper III). We also show in Table 5 the derived surface flux enhancements if $R = 1$. In Fig. 7 we show the modelled spectra for the individual stars and for the plages.

Some of the SWP line fluxes appear to be enhanced at phase 0.21 (SWP 21230). Assuming that this enhancement is related to the radio flare, we derived the flare spectrum shown in Fig. 7 by subtracting the G and K star global contributions from the $\phi = 0.21$ spectrum. Only the hottest lines (N v and C iv) are clearly visible in the flare spectrum. We discuss the flare further in Sect. 4.2.

The largest flux variation observed, in C II, is only 25%, so it is possible to attribute most, if not all, of the out-of-eclipse variability to uncertainties in measuring the IUE fluxes. However, we took every precaution in extracting and measuring the line fluxes and are confident that variations in excess of ~15% are significant. Without observations covering several orbits, it is not possible to separate secular variability from rotational modulation.

3.4. *The radio observations*

We obtained VLA observations on 4 and 5 October 1983 contemporaneously with those at other wavelengths. The VLA was split into 3 subarrays so that data could be obtained at 3 wavelengths – 2, 6, and 20 cm – simultaneously. These observations

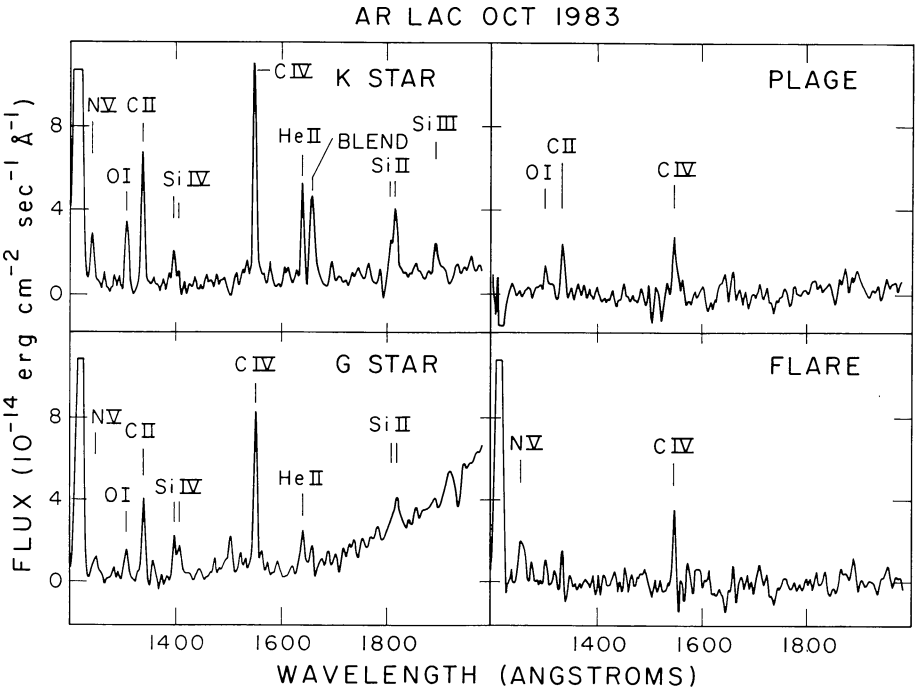

Fig. 7. The net SWP spectra for the individual stars and the plage and flare components. The plage spectrum shown was derived by assuming no limb brightening. Any limb brightening will *increase* the flux in the plage emission lines and *decrease* the flux in the K star emission lines. See Sect. 3.3 for a discussion of the assumptions we used to determine these component spectra

include the first detection of AR Lac at 2 cm. From 0232 to 0437 UT 4 October 1983 the source was relatively quiet, and no significant radio variability was seen. The flux densities at 1440 MHz (20 cm), 4860 MHz (6 cm), and 14960 MHz (2 cm) were 3 mJy, 15 mJy, and 11 mJy, respectively. On 5 October between 0230 and 1100 UT we detected the decay of a relatively large radio flare.

The radio flare (Fig. 8) is exceptional in several respects. First, the flare was *not* seen at 20 cm. This suggests that the emitting region lies below the optical depth unity surface at 20 cm and, thus, only the lower portion of the corona is involved in the radio flare. Secondly, the radio spectrum turned over between 2 and 6 cm (i.e., α became less than 0, where $S_\nu \sim \nu^\alpha$) during the decay phase of the flare. Inverted spectra are very rare in eclipsing RS CVn systems (Owen and Gibson, 1978), including AR Lac. The observation of such an optically thin spectrum suggests that there is little gas in this line of sight. Thirdly, some very rapid timescale variability ($\tau \lesssim 2$ min) in the form of "dips" occurred during the decay of the flare. These are particularly evident at 0410 and 0910 UT. They occur at both 2 and 6 cm but are deeper at the shorter wavelength. We have no explanation for these dips, although we note that they may be similar to the precipitous drop seen in the 1972 flare of Algol (Hjellming and Gibson, 1980).

We used the temporal, spectral, and polarization information from the flare to infer a number of coronal parameters in the flaring region. Assuming that the emission is synchrotron or gyrosynchrotron, consistent with other events of this type, and that the maximum in the observed spectrum ($\nu_{\max} \sim 5$ GHz) occurs near the critical frequency, we have

$$\nu_{\max} \gtrsim \nu_c = \frac{3eB}{4\pi m_e c} \gamma^2 \sin\psi , \tag{2}$$

where ψ is the pitch angle of the synchrotron electron (ψ is taken as 45°). Thus we infer that the local (average) B field and particle energies γ (the Lorentz factor) are related by

$$B\gamma^2 \lesssim 1700\,\mathrm{G} . \tag{3}$$

If the decay of the flare at 2 cm is due to synchrotron radiation losses, the time for the source flux to decay to half of its initial value is given by

$$\tau_{1/2} \approx 500\, B^{-2} (\gamma m_e c^2)^{-1} . \tag{4}$$

This leads to a second important inequality,

$$B^2\gamma \lesssim 3.4\,10^4\,\mathrm{G}^2 . \tag{5}$$

Solving Eqs. (3) and (5) for the two unknowns, we have

$$B \lesssim 90\,\mathrm{G} \text{ and } \gamma \gtrsim 4 . \tag{6}$$

These values for B and γ are typical of those found in other RS CVn flares (Hjellming and Gibson, 1980). The observed low-frequency spectral shape indicates that it is unlikely that Razin-Tsytovitch suppression occurs at wavelengths shorter than 30 cm. The Razin frequency is given as

$$\nu_r \sim \frac{2\nu_p^2}{3\nu_B} \sim \frac{20 n_e}{B \sin\psi} . \tag{7}$$

This relation leads to the inequality

$$\frac{n_e}{B} \lesssim 3.5\,10^7\,\mathrm{cm}^{-3}\,\mathrm{G}^{-1} \tag{8}$$

Using Eq. (6) to solve for n_e we obtain

$$n_e \lesssim 3\,10^9\,\mathrm{cm}^{-3} . \tag{9}$$

If the source became optically thin at 2 and 6 cm during the decay of the flare, we can estimate the particle energy spectral index Γ (such that $N[E] \propto E^{-\Gamma}$) from the relation $\alpha = -(\Gamma - 1)/2$, where α is the spectral index defined such that $S_\nu \propto \nu^\alpha$. This relation for α assumes the unlikely scenario that there is no evolution

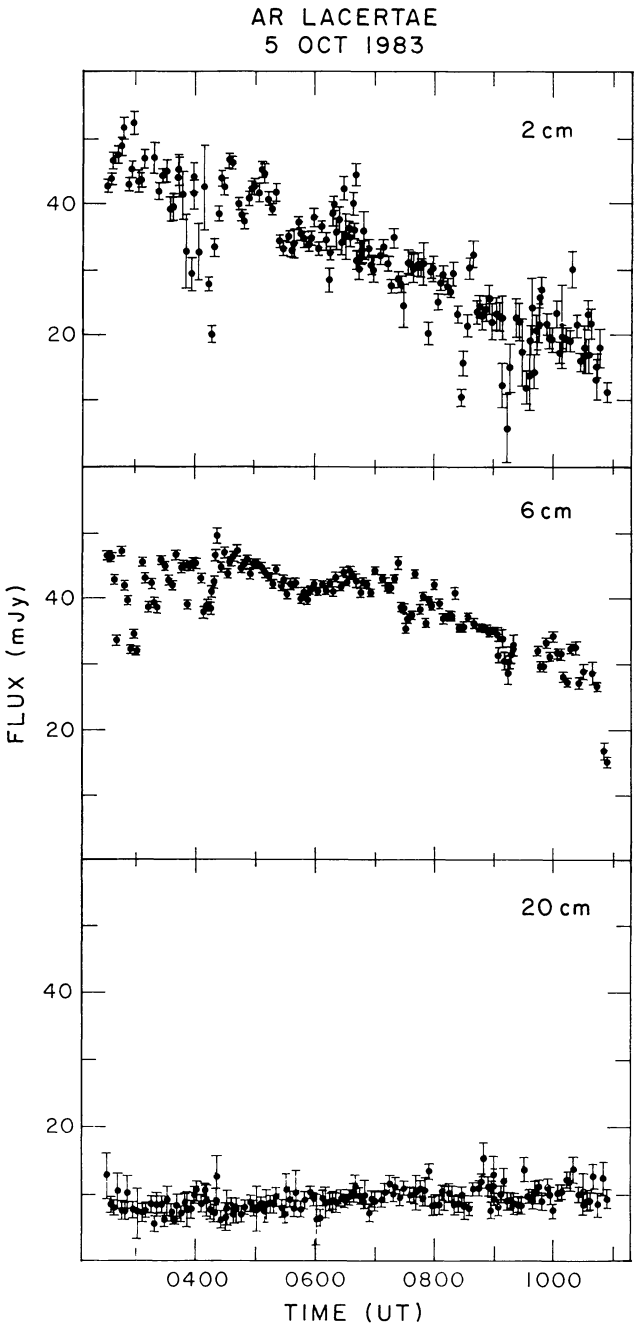

Fig. 8. Three frequency VLA observations of the large radio flare on 5 October. Note the lack of activity at 20 cm and the peculiar "dips" seen at 2 and 6 cm

of the particle energy spectrum. We doubt that the spectrum would evolve solely by synchroton losses (in which case $\alpha = (2\Gamma + 1)/3$), since collisional losses are also likely to be important, especially for the lower energy particles. For $\alpha = -0.5$, near the end of the observation, $\Gamma = 2$. This suggests that the flare produced a hard spectrum of relativistic particles, typical of that predicted for reconnection events. By following the analysis of Owen et al. (1976) we can use our estimate of Γ to infer the angular and, consequently, projected linear size of the radio emission region. The brightness temperature is given by $T_B = i_{\alpha 0}\gamma mc^2/k$, where $i_{\alpha 0}$ is a factor that depends on γ and Γ. For $\alpha \geq 4$ and $\Gamma = 2$, $i_{\alpha 0} \sim 0.4$ and $T_B \leq 10^{10}$ K. Given a distance of 40 pc to AR Lac, this implies that the size of the radio emitting region is $R_S \geq 0.75\, R_\odot$. The fact that no linear polarization was observed is consistent with the generally accepted hypothesis that any synchrotron-type emission would be Faraday depolarized over a relatively short length $L \sim 10^8$ cm, given the parameters determined above.

Although we have no simultaneous *VLBI* data, previous observations of this and other RS CVn systems suggest that the flaring plasma expands little if any, even during larger flares. This implies that the coronal dynamics are controlled by the magnetic field; i.e., the plasma $\beta = (8\pi n_e kT)/B^2 < 0.3$. Using our previously determined upper limits for n_e and B we can estimate the upper limit of the coronal temperature to be $T \lesssim 2.5\,10^8$ K.

4. Discussion of the surface features

4.1. The plages

The simplest explanation for the asymmetries of the K*k* line is the existence of regions of enhanced Mg II surface flux – i.e., plages – on the K star. Our data suggest the presence of at least two long-lived plages and one transient brightening of the K star.

The location and size of Plage B can be determined in a straightforward manner. Since the emission is unresolved in velocity, we make the assumption that the rotational velocity smearing is $\lesssim 10\,\mathrm{km\,s^{-1}}$. The spatial extent of the plage in longitude must therefore be less than $\sim 10°$. The longitude (345°) of the plage is well determined from the four observations. The latitude is more difficult to estimate. The amplitude of the observed radial velocity curve (see Fig. 9) is consistent with a location near the stellar equator. The observed $v \sin i = 90\,\mathrm{km\,s^{-1}}$ (relative to the K star) at $\phi = 0.19$ exceeds the photospheric $v \sin i$ slightly and is inconsistent with latitudes greater than about 20° If we assume that the plage is roughly circular, then its filling factor (fractional area coverage) is $\lesssim 0.005$ of the *visible* stellar

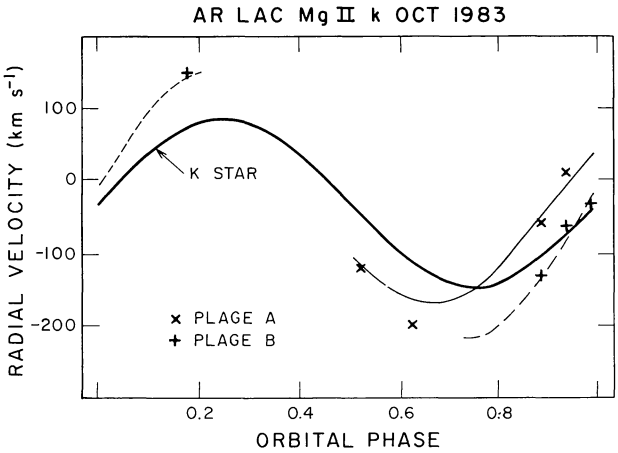

Fig. 9. Observed and predicted radial velocities of the plages. The thick line is the predicted radial velocity of the K star. The crosses mark the observed radial velocities of Plage A, and the pluses are the same for Plage B. The thin solid and dashed lines are the predicted velocities for features on the equator at stellar longitudes 280° and 345°, respectively. These lines are plotted only where the plage longitudes are on the visible hemisphere of the K star

hemisphere. Given this filling factor, the Mg II surface flux in the plage is at least five times larger than that of the mean K star surface flux.

The flux observed from Plage B remained constant to within 30% between $\phi = 0.88$ and 0.19. Although the limited phase coverage did not permit redetection of this plage on two successive rotations, the data suggest that it was not a short-lived, transient brightening.

The details of Plage A are somewhat more difficult to ascertain. This plage is most prominent at $\phi = 0.88$ (see Fig. 10a) as an asymmetry redward of the peak of the K*k* line. The residual emission has a resolved velocity width of $\sim 20\,\mathrm{km\,s^{-1}}$, implying resolved spatial extent of $\sim 20°$ in longitude (or a filling factor of 0.015), if the velocity width is due solely to geometrical effects and if the plage is circular.

The plage is present at $\phi = 0.93$, although it is nearly unmeasurable due to its proximity to the interstellar absorption. The plage position coincides with the wavelength of the absorption at $\phi = 0.97$. Because the interstellar absorption optical depth is constant, the equivalent width of the absorption should remain constant irrespective of the varying emission line profile. We have used this fact to establish the definite presence of plage emission at $\phi = 0.97$ and to estimate the flux in the plage at $\phi = 0.88$ and 0.93. The observed plage flux is $\sim 3\,10^{-13}\,\mathrm{erg\,s^{-1}\,cm^{-2}}$. If the plage is circular, then the Mg II contrast enhancement over the mean K star flux is comparable to that of Plage B.

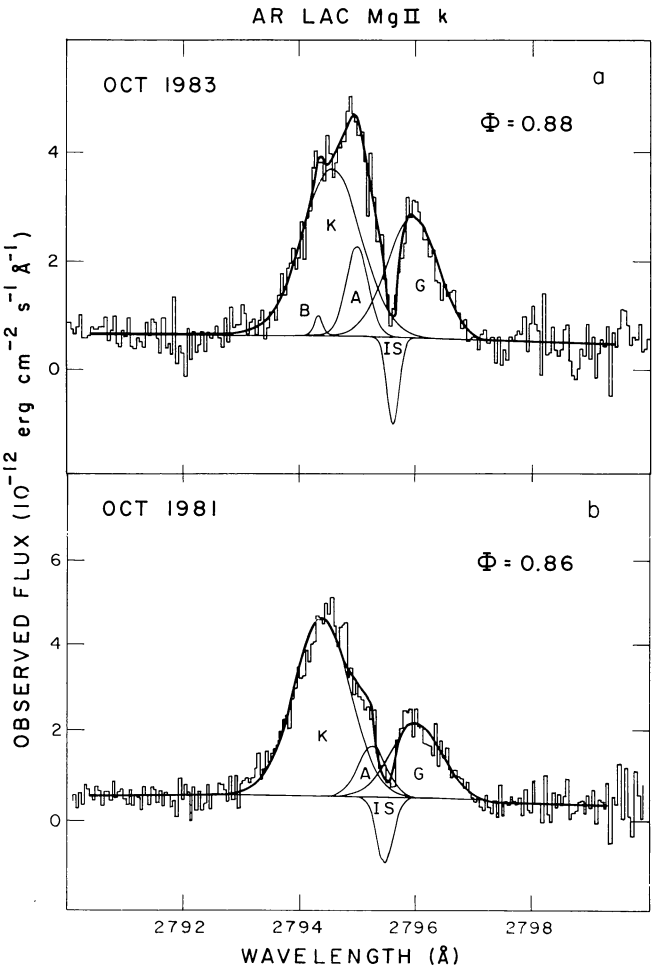

Fig. 10. a The Mg II *k* line profile at $\phi = 0.88$, showing both plages. The total flux in the plage components is about 10% of that in the global component at this phase. **b** A fit to the 1981 $\phi = 0.86$ profile requires at least four components to adequately model the global emission of the two stars. As in **a**, the plage component is needed to account for the asymmetry of the K star emission in the 1981 spectrum

The central wavelength of the emission from Plage A at $\phi = 0.88$ implies that its longitude is near 280°. This plage would be over the limb at $\phi = 0.19$ and 0.45 and should be visible again from $\phi = 0.51$ to 0.61. It is not clear that the plage reappeared; there is certainly far less contrast with the global K*k* line than there had been. There is a residual emission on the blue wing of the K*k* line at $\phi = 0.51$ at a velocity consistent with that expected from the plage but at $\sim 25\%$ of the expected flux. There is marginal evidence for the plage, again at roughly the proper velocity but at a much lower flux level, at $\phi = 0.61$, but no obvious plage was observed at $\phi = 0.56$. The enhanced K*k* flux at $\phi = 0.61$ (comparable to that at $\phi = 0.88$) might indicate that the plage redistributed itself over a much larger range in longitude, lowering its contrast with the surface while still contributing to the total K*k* flux.

The plage velocities indicate that they lie at or near the stellar photosphere. Heights greater than 0.2 stellar radii above the photosphere are inconsistent with the data shown in Fig. 9.

It is clear that the plages represent discrete areas of enhanced surface brightness, but they might undergo a substantial change in brightness or surface area on an orbital timescale. There is no evidence for comparable enhancements superimposed upon the fainter G-star profiles. The composite far-ultraviolet spectrum of the plages is presented in Fig. 7.

4.2. The transient brightening associated with the flare

There are four lines of evidence that lead us to conclude that there was a transient brightening of the chromospheric line fluxes associated with the radio flare. The radio emission was decaying at $\phi = 0.45$. We do not know when the radio flare began, or how bright it became, but if its decay timescale is consistent with previously observed flares, it might have begun before $\phi \sim 0.20$.

The first point concerns the K*k* line profile at $\phi = 0.19$, when the stellar profiles are most widely separated in this data set. At this phase the flux in the K*k* line is enhanced by nearly 50% over that seen at all other phases (except for $\phi = 0.61$; see discussion in Sect. 4.1). It is possible to attribute this excess flux to a transient brightening near disk center associated with the observed radio flare, because a bright spot with a velocity centroid near that of the K star and a broadening comparable to the stellar $v \sin i$ cannot be deconvolved unambiguously from the quiescent stellar profile. We therefore refit the Mg II *k* profiles obtained at phase 0.19 by constraining the K*k* line flux and width to be near the mean of the values observed at the other phases. The fit obtained is acceptable (Fig. 11), but it is not quantitatively superior to the original fit shown in Fig. 1. The residual emission is broad, corresponding to turbulent motions of $85\,\mathrm{km\,s^{-1}}$ ($T \cong 10^{6.5}$ K). This width indicates that the Mg II broadening is not of thermal origin. In light of the evidence for a radio flare, this broad emission component might indeed be real, and the most likely explanation is that it is due to turbulent motions or flows in the lower chromosphere that were associated with the coronal radio flare.

The second piece of evidence is the prominent enhancement on the red wing of the K*k* line seen at phase 0.45. The radial

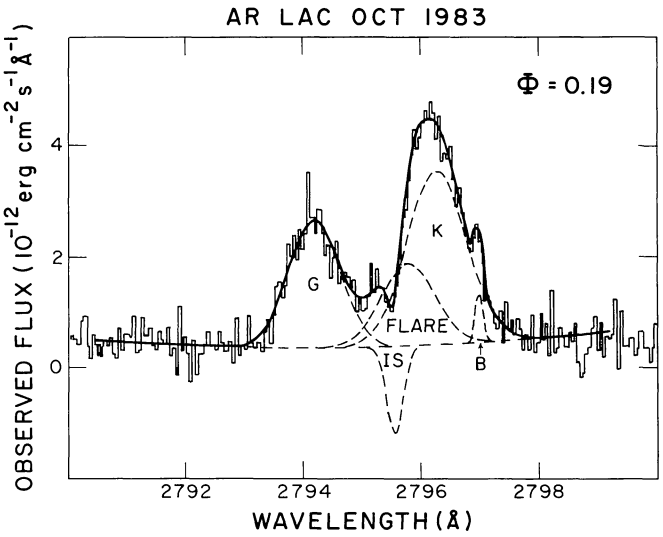

Fig. 11. Fit to the Mg II k line profile at $\phi = 0.19$, where we constrained the width and amplitude of the global K-star component to be the mean of the values determined at other phases in order to reveal the flare component. The flare component is quite broad, indicating velocities of order 85 km s^{-1}. Compare with Fig. 1

velocity is consistent with a bright spot that would have been near disk center at $\phi = 0.19$, and its flux is lower at this phase (by about an order of magnitude) than the excess in the Kk line at $\phi = 0.19$. This observation is consistent with a decaying transient associated with the radio flare and the $\phi = 0.19$ Kk enhancement.

The third point is that there is no evidence for any plage or enhancement on the blue wing of the Kk line at $\phi = 0.97$, as would be expected if the phase 0.45 enhancement is due to a long-lived plage. Since at phase 0.97 the blue wing of the Kk line is clear of the eclipse and the interstellar absorption, an enhancement with flux comparable to that seen at $\phi = 0.45$ would have been easily measurable.

Finally, the SWP spectrum obtained at phase 0.21 appears to show a slight enhancement in the lines of C IV and N V once the G and K star fluxes determined at eclipse are subtracted. Although previous observations of flares on AR Lac (Walter et al., 1984) indicated that the hot lines decay much faster than the cooler lines, the hot lines are also enhanced by much greater factors. A likely scenario is that the flare spectrum shown in Fig. 7 is the remnant of a flare that began one to two hours before this observation. This would place the previous LWR observation ($\phi = 0.19$) closer in time to the actual flare, explaining the higher enhancement at Mg II.

We conclude that a large flare occurred on the trailing hemisphere of the K star (near longitude 90°) at about 1200 UT on 4 October 1983. This flare caused a 50% increase in the Mg II emission flux from the K star. The radio emission and the Mg II flux were still decaying 13 h later.

4.3. Comparison with previous results

Figure 12 is a scale drawing of the AR Lac system. We have included our best estimate of the surface brightness distribution of the lower chromosphere of the K star. We note that the plages occupy the same hemisphere as that occupied by the extended component of the X-ray corona in 1980 (WGB). If the migration period of the photometric wave in AR Lac is about 12.5 yr (WGB), the active hemisphere might be expected to have rotated one quarter of the way around the star between 1980 and 1983. However, WGB argued that the photometric wave in this system is likely due primarily to the G star. The WGB 1980 X-ray data are in agreement, since the dark hemisphere at that epoch coincided with the X-ray bright hemisphere of the G star and the quiet hemisphere of the K star.

Since the limited phase coverage of the October 1983 data set left some uncertainty regarding the longevity of Plage A, we analyzed a spectrum obtained with IUE in October 1981 at $\phi = 0.86$ and reprocessed by NASA/IUE with the current software so that we could compare them with the October 1983 data (see Fig. 10b). The two line profiles are very similar, suggesting that Plage A was present at the time. More recent data, obtained in 1985 (Neff et al., 1986b) also show similar line profiles at this phase. Thus, we conclude that the emission we attribute to Plage A is due to a long-lived region of stellar activity. A detailed comparison of the surface structure at different epochs will be the subject of a later paper in this series.

We conclude that the active hemisphere of the K star remained fixed relative to the binary system from 1980 throughout 1983 and is independent of the photometric phase of the system if the migration rate is as fast as WGB claimed. This hypothesis can

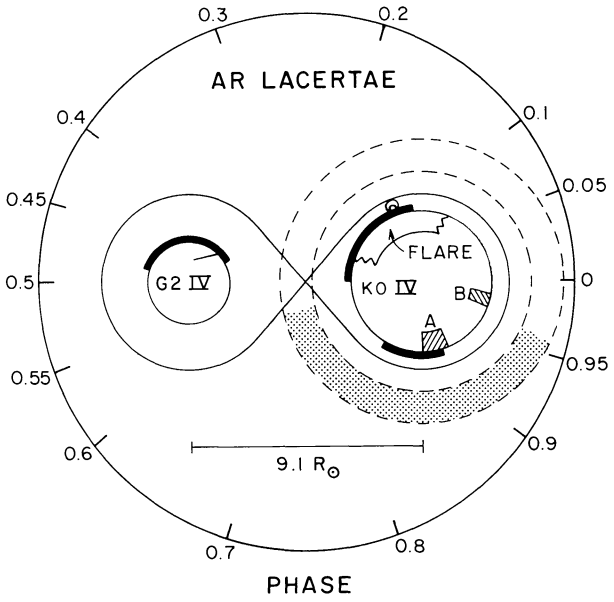

Fig. 12. The three discrete components observed in October 1983 (Plage A, Plage B, and Flare) are compared with the picture derived by WGB based on X-ray and UV observations in June 1980 (their Fig. 9). The solid line surrounding both stars represents the Roche surface. The thick solid line indicates the location of bright X-ray emission in the low corona, and the dashed lines surrounding the K star indicate the inner and outer radii (1.5 and 2.0 R_K) of the extended component of the K-star corona both seen in June 1980. The flaring loop also seen in June 1980 at $\phi \sim 0.30$ is not drawn to scale ($R_{loop} \lesssim 0.05\,R_K$). Note the similar longitudes of the flaring regions in 1980 and 1983 and of the plages with that of the active hemisphere of the K-star extended corona. The longitudinal extent of the 1983 flaring region is shown as an upper limit based upon the first and last observations of it. The flare component on the Mg II k line profile at $\phi = 0.45$, however, indicates that the region is probably compact ($\lesssim 20°$)

Table 6. AR LAC K star: properties of the extended coronal component

	WGB	This paper
n_e (cm^{-3})	$2.9\,10^9$	$\lesssim 3.0\,10^9$
T_e (K)	$3.0\,10^7$	$\leq 2.5\,10^8$
$R_{\rm eff}$[a]	0.85	≥ 0.75

[a] $R_{\rm eff}$ is the equivalent radius perpendicular to the line of sight of the coronal source in units of the stellar radius.

be tested by examining the IUE archival data as well as by obtaining new observations. If true, this will affect our understanding of differential rotation and of the mechanisms responsible for creating and sustaining localized activity. We also note that the location of the flare is near the location inferred by WGB for their flaring loop, although this could be coincidental.

The coronal parameters derived from the radio observations are consistent with those determined for the extended component of the K star corona by WGB during their X-ray eclipse observations of this system in 1980 (see Table 6). This similarity, together with the conclusion that the active hemisphere of the K star has remained about the same over the 3.3 yr interval, allows us to conclude that the radio emission probably arose from this extended coronal component. Using the parameters derived by WGB, we can calculate the free-free optical depth at each of the three frequencies,

$$\tau_\lambda = \int_L \mu(\nu)\, dl, \tag{10}$$

where $\mu(\nu) = 0.018 Z^4 N_e N_z g_{ff}(\nu, T)/\nu^2 T^{3/2}\,\mathrm{cm}^{-1}$, $g_{ff} = (3^{1/2}/\pi)\cdot \log(2.2kT/h\nu)$ as given by Tucker (1975), and $L = 5\,R_\odot$ is the line-of-sight thickness of the K star corona as viewed at the time of the flare. We find $\tau_{2\,\mathrm{cm}} = 0.026$, $\tau_{6\,\mathrm{cm}} = 0.26$, and $\tau_{20\,\mathrm{cm}} = 3.05$, consistent with our earlier conclusion that the flaring region lies below the optical depth unity surface at 20 cm. We note further that the plasma $\beta \gtrsim 0.12$ is consistent with a magnetically bound corona well beyond the Roche surface.

4.4. Caveats

Spatially resolved spectra, which can be derived from the variations in the SWP line fluxes in concert with spatial information from the Mg II Doppler imaging, can be used to generate multi-component atmospheric models that must be more realistic than simple uniform model atmospheres.

Our results provide several useful insights and constraints concerning the construction of multiple-component atmospheric models. First, observations of active stars must be made in as many different spectral regions as possible. This is necessary to understand the relationships of spots, plages, and flares. In addition, full and uniform phase coverage should be obtained. Further, this coverage should extend over more than one orbital cycle in order to confirm the longevity of the observed structures. The data set we have presented falls short on these last two counts, as the coverage was sparse and clustered near the eclipses (we had originally intended to make use of the occultation method of mapping structures) and extended over somewhat less than one orbit. We have recently obtained a more complete data set with continuous coverage of 90% of an orbit (Neff, et al., 1986b).

The conclusions we have presented are based on the *simplest self-consistent explanation* of the Mg II line profiles and the radio and UV fluxes as a function of time. Our scenario is not unique; more elaborate models with more free parameters might provide better fits to the data. The major drawback of this data set is the poor coverage near quadrature, when the lines are well separated and most amenable to analysis by our Doppler imaging technique. The 1981 data (Paper III) show features near quadrature that might be inconsistent with our model *if the surface features remained substantially unchanged over the two-year interval.* We suspect that, upon proper examination, the AR Lac system will prove more complex than we have concluded here.

5. Summary

We have demonstrated that it is possible to deconvolve discrete emission features from the composite Mg II *k* profiles of AR Lac using Doppler imaging techniques. Using the Doppler imaging results and the eclipse modulation, we were also able to determine the spectra of the two plages and a chromospheric brightening that was related to the radio flare. The velocities of these features and their Mg II *k* profiles allowed us to locate them on the surface of the K star and to determine their fractional area coverages and line surface fluxes. These data will permit us to determine the atmospheric structure within the plage regions alone. The Mg II surface flux enhancement in the plages relative to the mean (global) emission is roughly a factor of 5. The surface flux enhancement appears to be a maximum for the moderate temperature lines of O I and C II. We are using this information, along with observations obtained at other epochs and other wavelengths, to construct multiple-component atmospheric models for AR Lac at all heights (photosphere to corona) and over a long timescale.

Acknowledgements. We wish to thank K.G. Carpenter for assisting with the observations and P.B. Byrne, S. Catalano, and S.H. Saar for enlightening discussions. This research was supported by National Aeronautics and Space Administration grants NAG5-429 and NAG5-82 to the University of Colorado, CNR-GNA grant to the Catania Astrophysical Observatory, CNR-PSN and "Ministero della Pubblica Istruzione" grants to the Astronomy Institute of Catania University, and a travel grant (no. 386/84) from the NATO Scientific Affairs Division to maintain the collaboration between Armagh, Boulder, and Catania groups. The IUE data were analyzed using the facilities of the Colorado Regional Data Analysis Facility, which is supported by National Aeronautics and Space Adminstration grant NAG5-26409 to the University of Colorado. We thank the staffs of the IUE observatory and the Colorado RDAF for their assistance.

References

Ayres, T.R.: 1980, in *The Universe at Ultraviolet Wavelengths: The First Two Years of IUE*, p. 237, ed. R.D. Chapman, NASA-CP2171

Batten, A.H., Fletcher, J.M., Mann, P.J.: 1978, *Publ. Dom. Astrophys. Obs.*, **15**, 121

Bevington, P.R.: 1969, Data Reduction and Error Analysis for the Physical Sciences, McGraw-Hill, New York

Bielicz, E., Glebocki, R., Sikorski, J.: 1985, *Astron. Astrophys.* **153**, 269
Blanco, C., Catalano, S.: 1970, *Astron. Astrophys.* **4**, 482
Boggess, A. et al.: 1978, *Nature* **275**, 372
Bohlin, R., Holm, A.: 1980, *NASA IUE Newsletter* **10**, 37
Böhm-Vitense, E.: 1981, *Astrophys. J.* **244**, 504
Bray, R.J., Loughhead, R.E.: 1965, in *Sunspots*, Wiley and Sons, New York
Byrne, P.B., Doyle, J.G., Brown, A., Linsky, J.L., Rodonò, M.: 1987, *Astron. Astrophys*, **180**, 172 (Paper VI)
Cassatella, A., Ponz, D., Selvelli, P.L.: 1982, *ESA IUE Newsletter* **15**, 43
Chambliss, C.R.: 1976, *Publ. Astron. Soc. Pacific* **88**, 762
Crutcher, R.M.: 1982, *Astrophys. J.* **254**, 82
Eaton, J.A., Hall, D.S.: 1979, *Astrophys. J.* **227**, 907
Eddy, J.A.: 1979, *The New Sun: the Solar Results from Skylab*, NASA-SP102
Gibson, D.M., Hjellming, R.M.: 1974, *Publ. Astron. Soc. Pacific* **86**, 652
Hall, D.S.: 1976, in *Multiple Periodic Variable Stars*, IAU Coll. #29, ed. W.S. Fitch, Reidel, Dordrecht, p. 287
Hall, D.S.: 1981, in *Solar Phenomena in Stars and Stellar Systems*, eds. R. Bonnet and A. Dupree, Reidel, Dordrecht, p. 431
Hjellming, R.M., Gibson, D.M.: 1980, in *Radio Physics of the Sun*, eds. M.R. Kundu and T.E. Gergely, Reidel, Dordrecht, p. 209
Hoffleit, D.: 1982, *The Bright Star Catalog*, 4th Ed., Yale, New Haven
Kron, G.E.: 1947, *Publ. Astron. Soc. Pacific* **59**, 261
Linsky, J.L., Brown, A., Marstad, N.C., Rodonò, M., Andrews, A.D., Butler, C.J., Byrne, P.B.: 1984, in *Proc. Fourth European IUE Conference*, ESA-SP218, p. 351
Marstad, N., Linsky, J.L., Simon, T., Rodonò, M., Blanco, C., Catalano, S., Marilli, E., Andrews, A.D., Butler, C.J., Byrne, P.B.: 1982, in *Proc. Symp. on Advances in Ultraviolet Astronomy: Four Years of IUE Research*, NASA-CP2238, p. 554
Naftilan, S.A., Aikman, G.C.L.: 1981, *Astron. J.* **86**, 766
Naftilan, S.A., Drake, S.A.: 1977, *Astrophys. J.* **216**, 508
Neff, J.E., Gibson, D.M., Walter, F.M.: 1986a, in *Cool Stars, Stellar Systems, and the Sun*, eds. M. Zeilik and D.M. Gibson, Springer-Verlag, New York, p. 244
Neff, J.E., Walter, F.M., Rodonò M.: 1986b, in *New Insights in Astrophysics Based on Eight Years of IUE Research*, ESA SP-263, p. 153
Owen, F.N., Jones, T.W., Gibson, D.M.: 1976, *Astrophys. J. Letters* **210**, L27
Owen, F.N., Gibson, D.M.: 1978, *Astron. J.* **83**, 1488
Poe, C.H., Eaton, J.A.: 1985, *Astrophys. J.* **289**, 644
Popper, D.M., Ulrich, R.K.: 1977, *Astrophys. J. Letters* **212**, L131
Rodonò, M.: 1983, *Adv. Space Res.* **2**, No. 9, 225
Rodonò, M.: 1986, in *Cool Stars, Stellar Systems, and the Sun*, eds. M. Zeilik and D.M. Gibson, Springer-Verlag, New York, p. 475
Rodonò, M., Cutispoto, G. Pazzani, V., Catalano, S., Byrne, P.B., Doyle, J.G., Butler, C.J., Andrews, A.D., Blanco, C., Marilli, E., Linsky, J.L., Scaltriti, F., Busso, M., Cellino, A., Hopkins, J.L., Okazaki, A., Hayashi, S.S., Zeilik, M., Elston, R., Henson, G., Smith, P., Simon, T.: 1986, *Astron. Astrophys.* **165**, 135 (Paper I)
Rodonò, M., Byrne, P.B., Neff, J.E., Linsky, J.L., Simon, T., Catalano, S., Cutispoto, G., Doyle, J.G., Andrews, A.D., Gibson, D.M.: 1987, *Astron. Astrophys.* **176**, 267 (Paper III)
Simon, T., Herbig, G., Boesgaard, A.M.: 1985, *Astrophys. J.* **293**, 551
Soderblom, D.R.: 1985, *Publ. Astron. Soc. Pacific* **97**, 57
Stencel, R.E., Mullan, D.J., Linsky, J.L., Basri, G.S., Worden, S.P.: 1980, *Astrophys. J. Suppl.* **44**, 383
Swank, J.H., White, N.E., Holt, S.S., Becker, R.H.: 1981, *Astrophys. J.* **246**, 208
Tucker, W.H.: 1975, in *Radiation Processes in Astrophysics*, MIT, Cambridge
Vogt, S.S.: 1983, in *Activity in Red Dwarf Stars*, IAU Coll. #71, eds. P.B. Byrne and M. Rodonò, Reidel, Dordrecht, p. 137
Vogt, S.S., Penrod, G.D.: 1983, *Publ. Astron. Soc. Pacific* **95**, 565
Walter, F.M., Cash, W., Charles, P.A., Bowyer, C.S.: 1980, *Astrophys. J.*, **236**, 212
Walter, F.M., Gibson, D.M., Basri, G.S.: 1983, *Astrophys. J.* **267**, 665 (WGB)
Walter, F.M., Gibson, D.M., Brown, A., Carpenter, K., Linsky, J.L., Rodonò, M., Eyles, C.: 1984, *Bull. Amer. Astron. Soc.* **16**, 896